Materials Research Express

RECEIVED
21 December 2018

REVISED
4 April 2019

ACCEPTED FOR PUBLICATION
15 April 2019

PUBLISHED
24 April 2019

PAPER

Direct observations of multi-cyclic nanoindentation-induced phase transformations in single-crystal Ge

Koji Kosai and Jiwang Yan

Department of Mechanical Engineering, Faculty of Science and Technology, Keio University, Hiyoshi 3-14-1, Kohoku-ku, Yokohama 223-8522, Japan

E-mail: yan@mech.keio.ac.jp

Keywords: single-crystal germanium, nanoindentation, cyclic load, phase transformation, subsurface damage, microstructural change, mechanical processing

Abstract

Multi-cyclic nanoindentation experiments with various holding loads were carried out on single-crystal Ge to investigate pressure-induced phase transformation behaviors. Cross-sectional transmission electron microscopic observation and laser micro-Raman spectroscopy of the indents revealed various phase transformation behaviors at different holding loads. Distinctive phase transformation behaviors were observed under various loading and unloading conditions. With a low holding load, a broad phase transformed region containing r8-Ge phase and dislocations was generated. A middle holding load promoted twinning but limited phase transformations. On the other hand, a densely transformed region containing dc-Ge, a-Ge, r8-Ge and st12-Ge was widely formed at a high holding load. In addition, the calculation results of the average contact pressure in the last unloading step verified the occurrence of these phase transformations. By integrating these results, a path diagram for phase transformations of single-crystal Ge during multi-cyclic nanoindentation was established, which is useful for understanding the subsurface damage formation in mechanical processing of the material.

1. Introduction

Single-crystal germanium (Ge) exhibits diverse phase transformation behaviors at a high pressure. Stable diamond cubic structure (dc-Ge) transforms to a metallic phase so called (β-Sn)-Ge by high pressure [1–4]. The metallic phase is unstable and demonstrates further phase transformation on the subsequent pressure release. The end phases possess significantly different properties. Hence, revealing the phase transformation mechanism during loading/unloading processes helps to optimize the mechanical machining and surface processing of Ge. This will improve the productivity and surface integrity of Ge substrates which are widely used as infrared (IR) optical elements and semiconductor devices.

Phase transformation behaviors in single-crystal Ge have been extensively studied by nanoindentation and diamond anvil cell (DAC) experiments. In previous research, various factors determining phase transformation behaviors have been reported. For example, pressure change speed is identified as a critical factor to determine end phases [5–8]. In a DAC experiment, fast decompression generated a body-centered cubic Ge (bc8-Ge), whereas slow decompression formed a simple tetragonal Ge (st12-Ge) [5]. On the other hand, a nanoindentation study reported that fast depressurization resulted in st12-Ge phase [6]. This inconsistency was explained by considering stress conditions [6, 9]. Another DAC experiment revealed the stress dependence of phase transformation in Ge; the hydrostatic pressure caused a phase transformation to a rhombohedral phase (r8-Ge), while the shear stress resulted in st12-Ge [9]. Based on the nanoindentation experiment of amorphous Ge (a-Ge), phase transformation pathways from (β-Sn)-Ge were classified into two types depending on the stress conditions [6].

In addition to phase transformation, defect nucleation and propagation has also been found in nanoindentation using a sphere indenter [10] and at slow loading/unloading rates [7]. In such a situation, phase

Table 1. Indentation conditions in this study.

	Single mode	Multi-cyclic mode
Maximum load (mN)	50	50
Loading/unloading rate (mN s^{-1})	50	50
ΔP (mN)	No value	2, 14, 50
Holding time of maximum load (s)	1	1
Holding time of ΔP (s)	No value	5

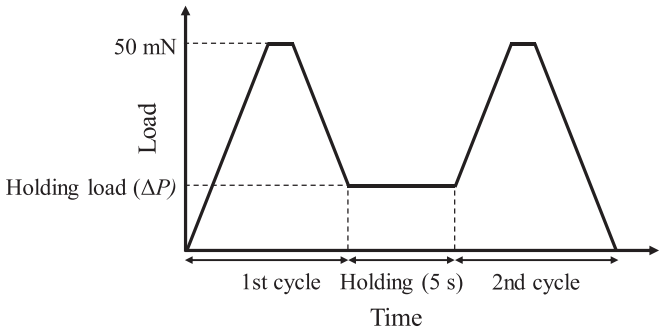

Figure 1. Indentation procedure for multi-cyclic nanoindentation.

transformation was prevented by crystal defects, especially twins [7]. The influence of crystal defects can be eliminated by indentation of a-Ge. Some previous studies revealed interesting phase transformation behaviors in indentation of a-Ge, whereas single-crystal Ge demonstrated both phase transformation and defect nucleation [11–13]. In particular, multi-cyclic nanoindentation induced complicated behaviors due to repetitive pressure [14–16]. In fact, single-crystal silicon (Si), which possesses similar crystal properties to Ge and also shows pressure-induced phase transformation [1–4, 14, 17–27], demonstrated interesting phase transformations during multi-cyclic nanoindentation [14, 26–29]. For single-crystal Ge, Kosai *et al* recently attempted multi-cyclic nanoindentation tests and found unique phase transformation behaviors which have never been reported for a single indentation [15, 16]. However, up to date, the physics underlying the phase transformations in multi-cyclic nanoindentation of Ge is not clear, thus systematic comparative study is necessary to identify the phase transformation pathways depending on multi-cyclic loading and unloading conditions.

In this study, by applying a wide range of systematically designed conditions, different responses of single-crystal Ge during multi-cyclic nanoindentation were comparatively discussed. The subsurface material microstructural changes beneath the indented surface were directly observed by using cross-sectional transmission electron microscopy (TEM) in combination with laser micro Raman spectroscopy. The TEM observation results were then integrated with surface observation by using scanning electron microscopy (SEM) and pressure analysis by using average contact pressure (ACP). Based on these newly obtained direct evidences, a phase transformation path diagram was established. The findings from this study will provide deeper understanding of pressure-induced behaviors in Ge under complex loading/unloading conditions, which contributes to clarifying the subsurface damage formation mechanism and optimizing the conditions for the mechanical processing of Ge.

2. Experimental procedures

Nanoindentation tests were carried out on a single-crystal Ge (111) wafer by nanoindentation instrument ENT-1100a (Elionix Inc., Japan). In the instrument, a Berkovich indenter of single-crystal diamond was equipped. All indentation conditions applied in this study are shown in table 1. Multi-cyclic nanoindentation was performed by the procedure illustrated in figure 1. The holding load between the 1st and 2nd cycle was defined as ΔP. For $\Delta P =$ 50 mN, the indentation protocol can be regarded as a single nanoindentation with holding maximum load (50 mN) for 7 s. For comparison, single indentation was also performed.

After the indentation, the crystalinity of the residual indents was investigated by a laser micro-Raman spectrometer NRS-3000 (JASCO, Japan). The wavelength of laser used in the spectrometer was 532 nm and spot size was ~1 μm. Possible time-induced phase transformation of Ge [6, 8, 11, 30] after indentation may affect the results. To ignore the effect, the Raman analysis was performed within 3 h after indentation. After Raman

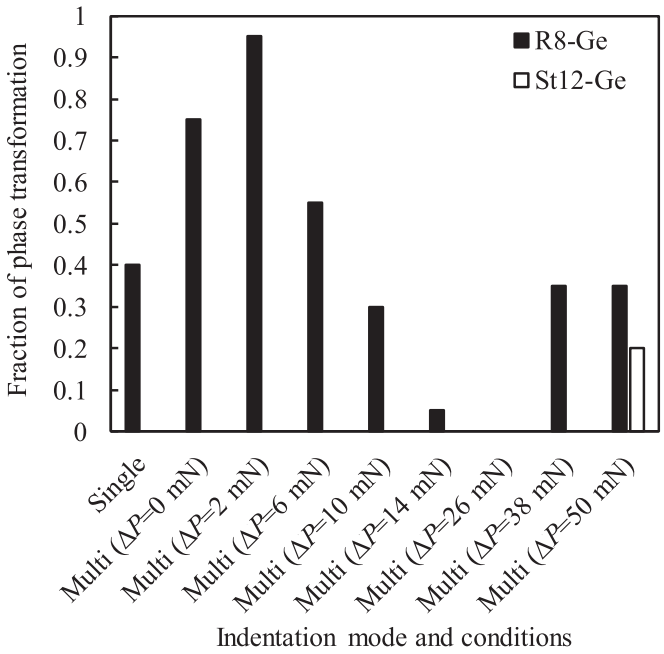

Figure 2. Fractions of phase transformation to r8-Ge or st12-Ge [15, 16].

analysis, the samples surfaces were further observed by SEM. Furthermore, an extremely thin (thickness around 90 nm) cross-sectional sample was made along an edge of the Berkovich indenter by using focused ion beam (FIB) machining, which was subsequently observed by using a TEM. The observation results were also compared with those obtained by single indentation tests.

To investigate the pressure change during indentation, ACP was calculated from indentation depth. In the calculation, the elastic deformation of surface is assumed to be proportional to the square root of the indentation load [31]. The analysis of ACP has been utilized to explore the pressure sensitive phase transformation of single-crystal Si [25, 26, 29].

3. Results and discussion

3.1. Raman analysis

Laser micro-Raman spectroscopy analysis showed that r8-Ge and st12-Ge were formed in different frequency depending on the holding load ΔP, as shown in figure 2 [15, 16]. The fraction in figure 2 represents the ratio of detecting r8-Ge or st12-Ge formed by phase transformation in 20 indents at each condition. The phase transformation to r8-Ge was promoted at a low ΔP, although the fraction was obviously decreased with increasing ΔP to 14 mN or 26 mN. For high ΔP (38 mN and 50 mN), however, the fraction increased. In addition, indentation with the highest ΔP of 50 mN caused st12-Ge formation. There was no detection of st12-Ge in other conditions. Although the fraction was only 0.2, the high ΔP would tend to generate larger shear stress than lower ΔP because st12-Ge formation needs shear stress [6, 9].

3.2. Surface SEM observation

Figure 3 shows typical SEM images of indent surfaces for single and multi-cyclic indentation with low (2 mN), middle (14 mN) and high (50 mN) ΔP with or without r8-Ge peaks on Raman spectra. As compared with the single indentation of (a) and (b), surface undulations and side extrusions are more obviously observed at multi-cyclic nanoindentation of (c) $\sim$ (h) regardless of ΔP or whether the r8-Ge peak appears on Raman spectra or not. The surface undulations and side extrusions might be caused by the flow of soft ductile (β-Sn)-Ge sandwiched by relatively harder surrounding dc-Ge and the diamond indenter [8, 32]. These observed results indicate that multi-cyclic indentation causes a larger plastic flow of (β-Sn)-Ge on the surface than single indentation. The plastic flow is formed by extruded (β-Sn)-Ge toward outside of indents during loading and holding. Hence, repetitive loading process and long holding process of multi-cyclic nanoindentation formed obvious undulation and extrusion. However, there is no difference in dependence on r8-Ge existence. The intermediate (β-Sn)-Ge transforms to not only r8-Ge and st12-Ge but also dc-Ge and a-Ge [6–8]. In the plastic flow, because of the dynamic and unstable stress transition, (β-Sn)-Ge transforms to such various end phases

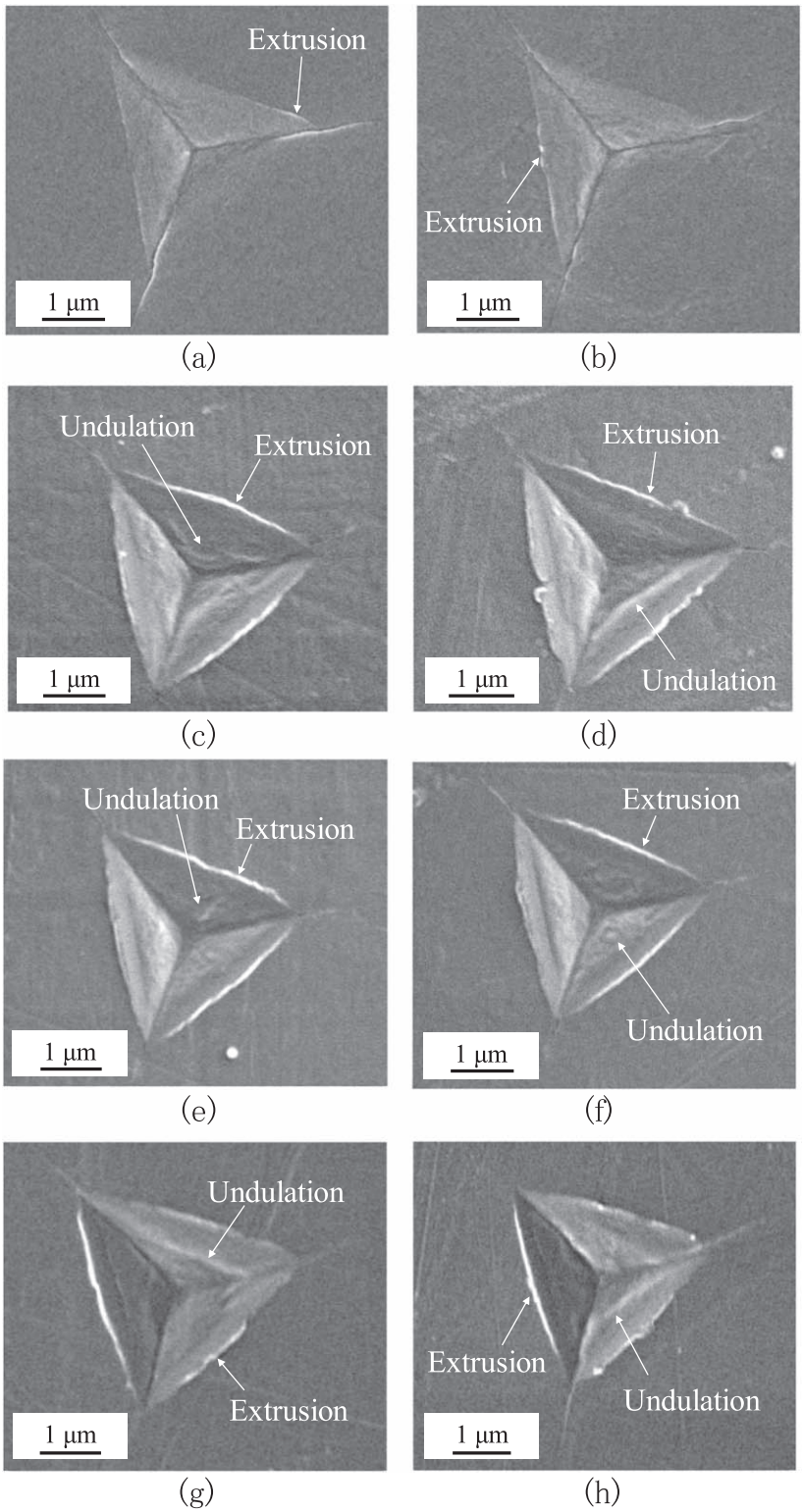

Figure 3. SEM images of indent surfaces; (a) single indentation with phase transformation to r8-Ge; (b) single indentation without phase transformation to r8-Ge; (c) $\Delta P = 2$ mN with phase transformation to r8-Ge; (d) $\Delta P = 2$ mN without phase transformation to r8-Ge; (e) $\Delta P = 14$ mN with phase transformation to r8-Ge; (f) $\Delta P = 14$ mN without phase transformation to r8-Ge; (g) $\Delta P = 50$ mN with phase transformation to r8-Ge; (h) $\Delta P = 50$ mN without phase transformation to r8-Ge.

and the amount of each phase is not enough to appear on Raman spectra. Therefore, the plastic flow is not an indication of end phases on Raman spectra. To reveal the different phase transformation mechanism depending on indentation conditions, behaviors beneath the surface should be investigated.

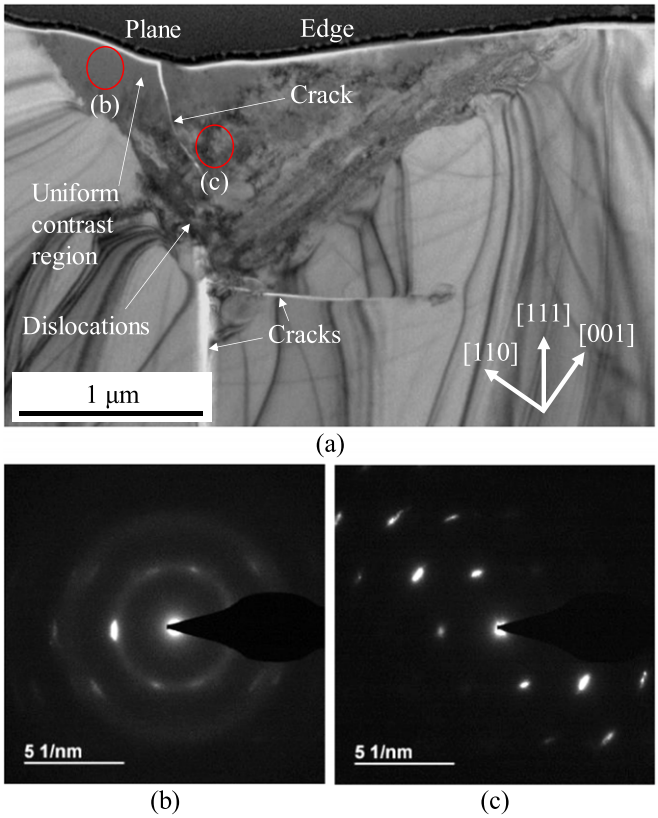

Figure 4. Cross-section and SADP of an indent at single mode observed by TEM; (a) TEM image; (b), (c) SADP at circles in (a).

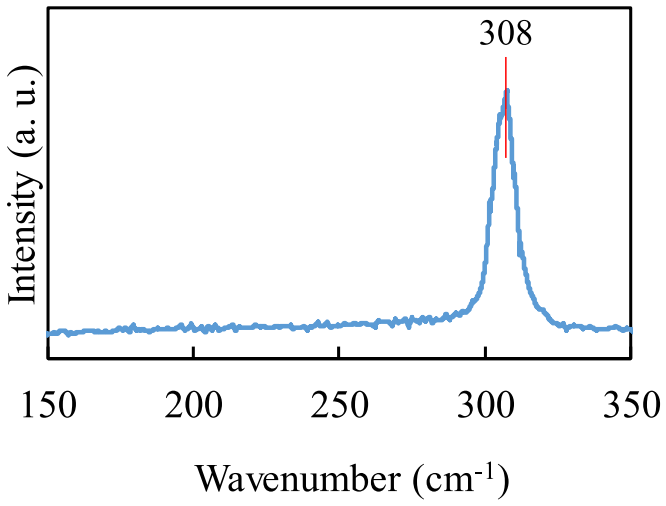

Figure 5. Raman spectrum obtained from the indent of figure 4.

3.3. Cross-sectional TEM observation

A cross-sectional TEM image of an indent obtained by single indentation is shown in figure 4(a). Figure 5 is the Raman spectrum of the indent. There is only a peak of dc-Ge around 308 cm^{-1} which shows a shift from the original location around 300 cm^{-1} due to compressive stress [10, 14]. Immediately underneath the indent in figure 4(a), a region of uniform contrast exists on the left side corresponding to a face of the indenter. Figure 4(b) is the selected area diffraction pattern (SADP) at the region. Not only some spots of initial dc-Ge phase, but also broad rings around the center corresponding to a-Ge are observed. However, the uniform contrast region showing a-Ge existence is obviously smaller than the whole affected region by the indentation in figure 4(a). In the right side which looks ununiform in contrast, no phase transformation could be detected, as shown in SADP

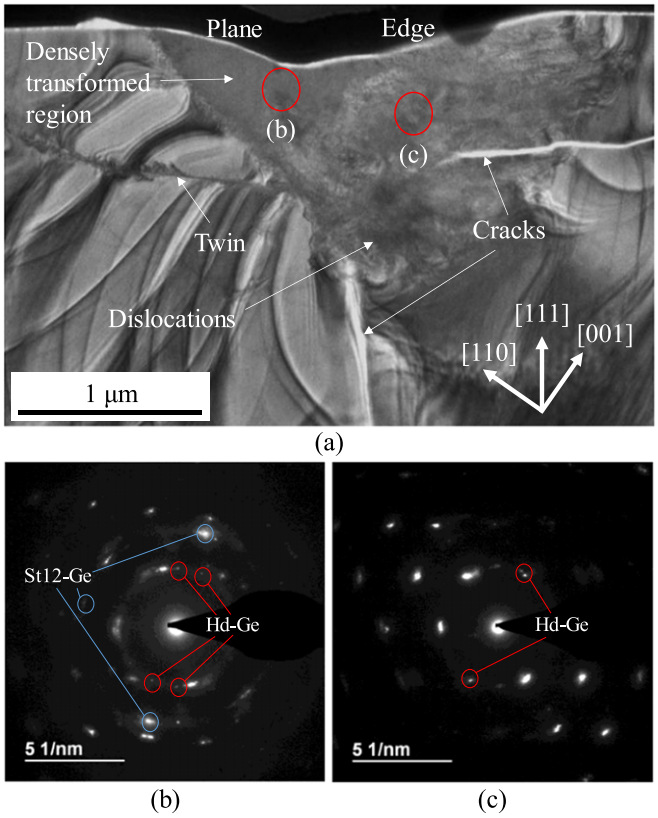

Figure 6. Cross-section and SADP of an indent with a ΔP of 2 mN observed by TEM; (a) TEM image; (b), (c) SADP at circles in (a) [16].

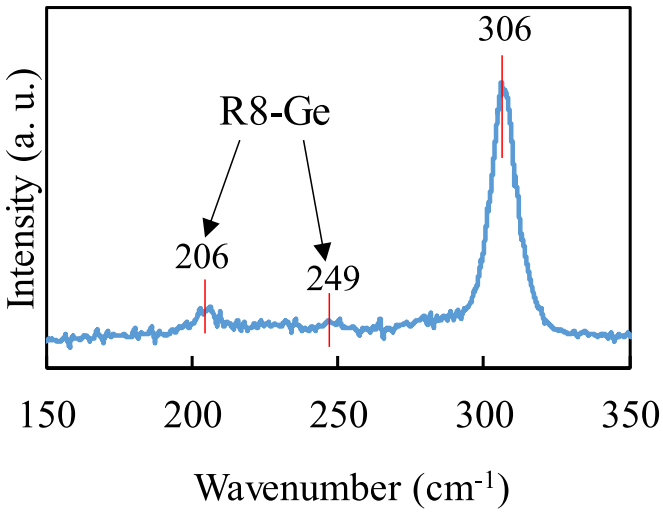

Figure 7. Raman spectrum obtained from the indent of figure 6 [16].

of figure 4(c). These results suggest that amorphization of Ge occurs only in a limitted region in single indentation.

Figure 6(a) is the result of TEM observation for multi-cyclic nanoindentation with a ΔP of 2 mN. The Raman spectrum obtained from the indent is illustrated in figure 7, where r8-Ge peaks appear around 206 cm^{-1} and 249 cm^{-1} [11, 30]. On the left side of figure 6(a), a region of uniform contrast exists with showing SADP in figure 6(b). In addition to broad rings of a-Ge, light spots of hexagonal diamond Ge (hd-Ge) and st12-Ge were also confirmed. The detected hd-Ge was transformed from r8-Ge formed by indentation before TEM observation because r8-Ge transforms to hd-Ge at room temperature after a few hours [6, 11, 30]. These results demonstrate that phase transformation from initial dc-Ge to different phases via (β-Sn)-Ge would densely occur

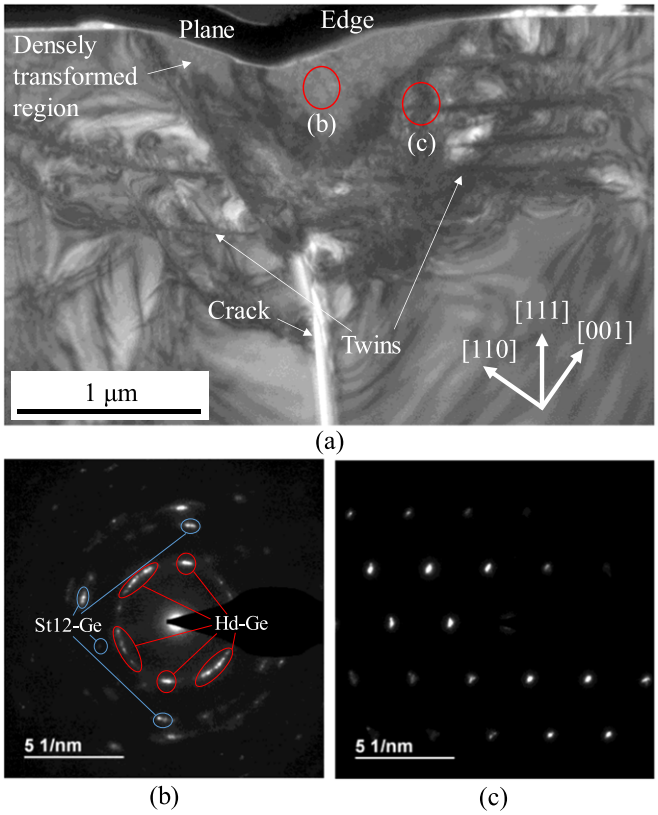

Figure 8. Cross-section and SADP of an indent with a ΔP of 14 mN observed by TEM; (a) TEM image; (b), (c) SADP at circles in (a) [16].

during indentation. It should be pointed out that it is difficult to distinguish hd-Ge on Raman spectra because hd-Ge shows a broad peak immediately beside the strong dc-Ge peak [11, 12, 30]. Phase transformation behaviors in this region may affect the difference of Raman spectra between figure 5 and figure 7. However, there is no detection of st12-Ge in figure 7 although the phase appeared on SADP in figure 6(b). Therefore, there should be other factors dominating the phase transformation difference in figure 2. On the right side of figure 6(a), which corresponds to an edge of the Berkovich indenter, a misty region exists widely. Especially in the dark region, dislocations are intensely generated, which was also confirmed at the single indentation in figure 4(a). However, SADP of figure 6(c) proves the existence of hd-Ge in the region. Therefore, r8-Ge should have been formed there, which is different from the single indentation in figure 4. This wide phase transformed region would result in the more frequent appearance of r8-Ge than other conditions in figure 2.

Figure 8(a) is the observed cross-section of an indent obtained by multi-cyclic nanoindentation with a ΔP of 14 mN. The indent showed a Raman spectrum in figure 9, where no phase transformation appeared. Around the tip of indent, a densely transformed region is formed like the case of $\Delta P = 2$ mN. Figure 8(b) shows st12-Ge and hd-Ge phases, although not visible in the Raman spectrum probably because it is a very small region. In the surrounding region, on the other hand, twins are generated widely as compared with figure 6(a). SADP around the twins represented no phase transformation as figure 8(c). As reported in [7], phase transformation may be prevented by twinning. In this experiment, twins similarly prevented phase transformation in the surrounding region. The holding process with a middle ΔP would accumulate a higher stress to the sample than that of a low ΔP. For single-crystal Si, either defect propagation or phase transformation will be promoted in such a case [24]. For single-crystal Ge, on the other hand, nucleation and propagation of twins would dominantly progressed under gradual pressuring due to strain rate sensitivity of Ge [7, 33]. Hence, gradual pressuring during the holding process prevented phase transformation by twinning as figure 8(c). As a result, phase transformation on the 2nd cycle would be narrowly limited, which caused the infrequent detection of r8-Ge on Raman spectra as shown in figure 2. For the case of a low ΔP, on the other hand, the holding process would not promote twinning due to small ΔP, and a wide phase transformed region was formed on the 2nd cycle as shown in figure 6(a). For single indentation, such significant twinning does not occur because there is no holding process, which results in the higher fraction in figure 2 than those of middle ΔP.

Figure 10(a) is a cross-sectional TEM image of an indent with a ΔP of 50 mN. The Raman spectrum of this indent is figure 11. In addition to r8-Ge, st12-Ge is detected by a weak peak around 280 cm^{-1} on the Raman

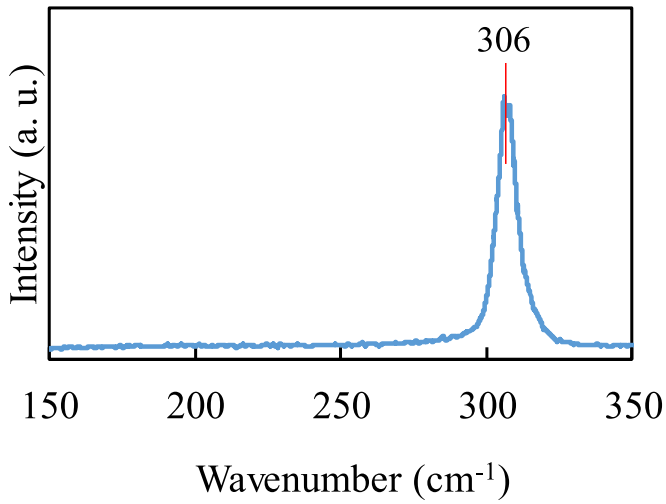

Figure 9. Raman spectrum obtained from the indent of figure 8 [16].

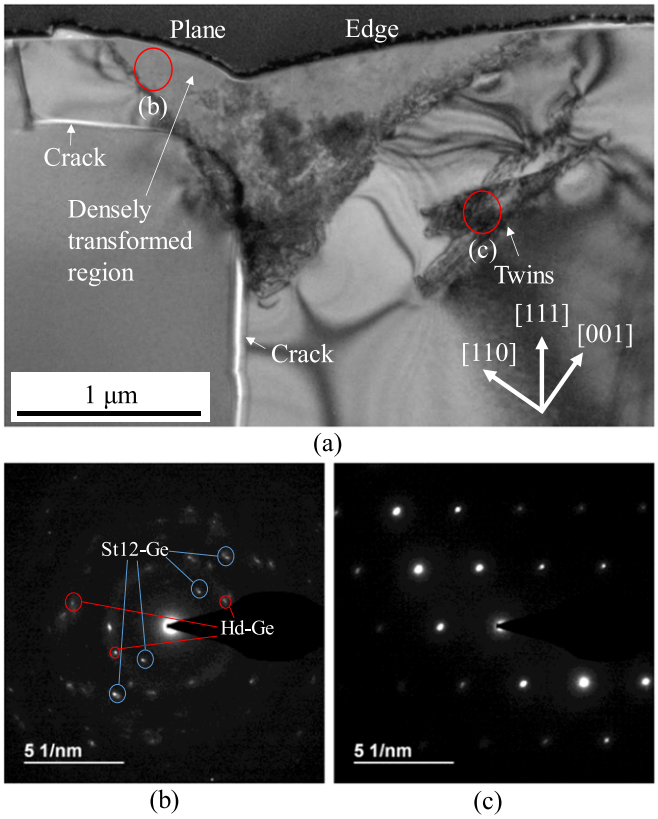

Figure 10. Cross-section and SADP of an indent with a ΔP of 50 mN observed by TEM; (a) TEM image; (b), (c) SADP at circles in (a) [16].

spectrum [7, 17]. Since st12-Ge is formed under shear conditions [6, 9], this indicates that a high ΔP of 50 mN caused higher shear stress than lower ΔP. Near the indented surface in figure 10(a), a densely phase transformed region exhibiting SADP in figure 10(b) is more widely formed than other conditions (figure 4, figure 6 and figure 8). By expansion of the densely transformed region, indentation with a high ΔP recorded the higher fraction of r8-Ge formation than a middle ΔP in figure 2. It should be mentioned that a misty region is smaller than that of a low ΔP in figure 6. This suggests that further phase transformation was suppressed by twinning at the outer region in figure 10(c) as the same as the case of a middle ΔP. This resulted in the less r8-Ge appearance than that of a low ΔP as shown in figure 2.

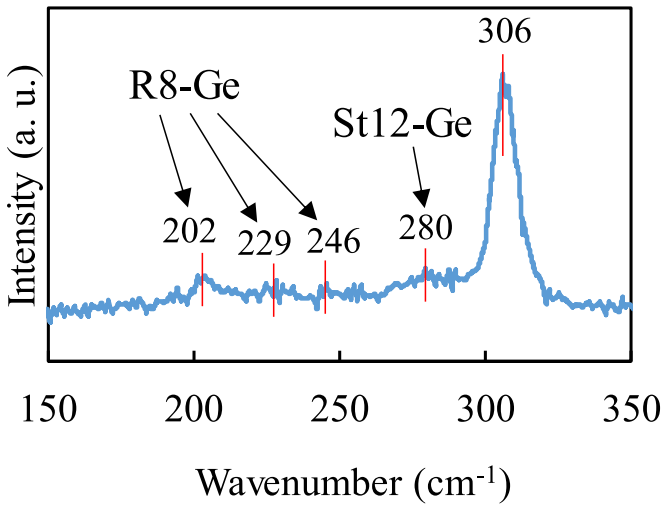

Figure 11. Raman spectrum obtained from the indent of figure 10 [16].

It should be noted that the non-repetitive loading/unloading process of indentation with a ΔP of 50 mN might also cause the difference from indentation with a low ΔP. However, the main factor forming the wide densely transformed region would be a holding process with a high ΔP. A path to form the densely transformed region can be explained as below. Dc-Ge transforms to (β-Sn)-Ge on the 1st loading process. At low and middle ΔP, this intermediate phase transformed to other phases before the holding process with releasing stress. At a high ΔP, on the other hand, the (β-Sn)-Ge was sustained because of little or no unloading before holding. As a result, high stress was accumulated to the sustained (β-Sn)-Ge during holding with a high ΔP. This wide layer of (β-Sn)-Ge with high stress transformed to the densely transformed region in figure 10(a) on the subsequent unloading. For single indentation, holding at the maximum load is short and only a little stress is accumulated. This results in a small transformed region in figure 4.

3.4. Loading/unloading characteristics

Figure 12 illustrates the load-displacement curves for each indentation of the TEM images in figures 6, 8 and 10. To clearly illustrate each cycle, an artificial shift is inserted between the 1st and 2nd cycles of figures 12(a) $\sim$ (c). In figure 12(c), a sudden displacement decreases so-called pop-out appears on unloading, whereas no pop-out appears on other curves. Some previous research indicated the correspondence between the pop-out and phase transformation for Si and Ge [14, 15, 20–23, 25–30, 34]. In this study, phase transformation to r8-Ge at the indentation with a high ΔP also presented the correspondence. Namely, r8-Ge was confirmed by Raman spectrometer only at indents showing pop-outs on the unloading processes. Phase transformation from (β-Sn)-Ge to other phases causes volume expansion [35]. Therefore, it is assumed that the wide densely transformed region in figure 10 would be formed by catastrophic phase transformation from intermediate (β-Sn)-Ge causing a momentary volume expansion at the pop-out.

Figure 13 illustrates the calculated ACP during each indentation of figure 12. In figure 13(a) corresponding to the indentation of Figure 6 ($\Delta P =$ 2 mN), a slight slope transition is observed at the ACP around 6 $\sim$ 7 GPa on the 2nd unloading process. This ACP corresponds to the phase transformation pressure from (β-Sn)-Ge to r8-Ge in a DAC experiment [9]. This fact indicates that before the slope transition, r8-Ge would be gradually formed on the 2nd unloading process by random nucleation and growth as reported for Si [34]. This process would end up the wide phase transformation in the surrounding region as confirmed in figure 6(a). The disconnected phase transformation causes gradual volume expansion since r8-Ge possesses a larger volume than (β-Sn)-Ge [36]. By the slope transition point, phase transformation to r8-Ge completes. As a result, the subsequent unloading process showed slower displacement decrease by elastic recovery without phase transformation. This caused the faster ACP decrease per displacement as compared with pre-slope-transition. On the 1st unloading process, on the other hand, the slope of ACP decrease is almost constant. This indicates that in addition to elastic recovery, phase transformation would continuously occur in the densely transformed region on the 1st unloading process. Stress at the region is higher than the surrounding region, so even at a low ACP, volume expansion by phase transformation continuously occurs.

For indentation with a middle ΔP, the slope of ACP decrease is almost constant on the 2nd unloading process in figure 13(b). This indicates that at a middle ΔP, constant elastic recovery is the dominant factor of displacement decrease since phase transformation is prevented by wide twinning. In the 1st unloading process,

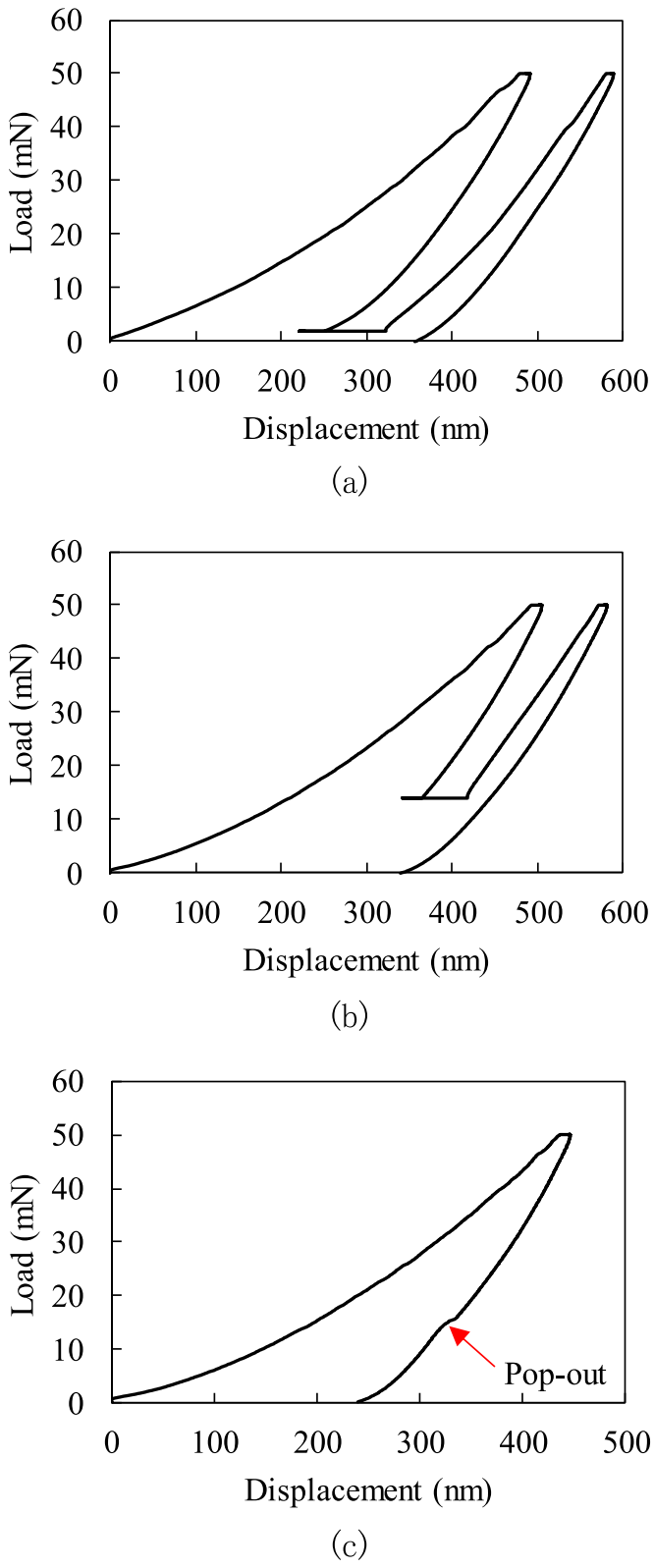

Figure 12. Load-displacement curves; (a) the indent in figure 6 ($\Delta P =$ 2 mN); (b) the indent in figure 8 ($\Delta P =$ 14 mN); (c) the indent in figure 10 ($\Delta P =$ 50 mN) (between the 1st and 2nd cycle, an artificial shift is inserted in (a) ~ (c)).

phase transformation resulting in the densely transformed region in figure 8(a) would occur, similar to indentation with a low ΔP. It should be noted that the slopes of the 1st and 2nd unloading process are almost the same. This suggests that phase transformation in the densely transformed region might be repeated even in the 2nd unloading process. To verify this possibility, further research is needed.

In figure 13(c), the pop-out clearly appears at the ACP of ~5 GPa on the unloading process. This ACP is lower than the pressure of phase transformation from (β-Sn)-Ge to r8-Ge or st12-Ge [9, 35]. Hence, it is well

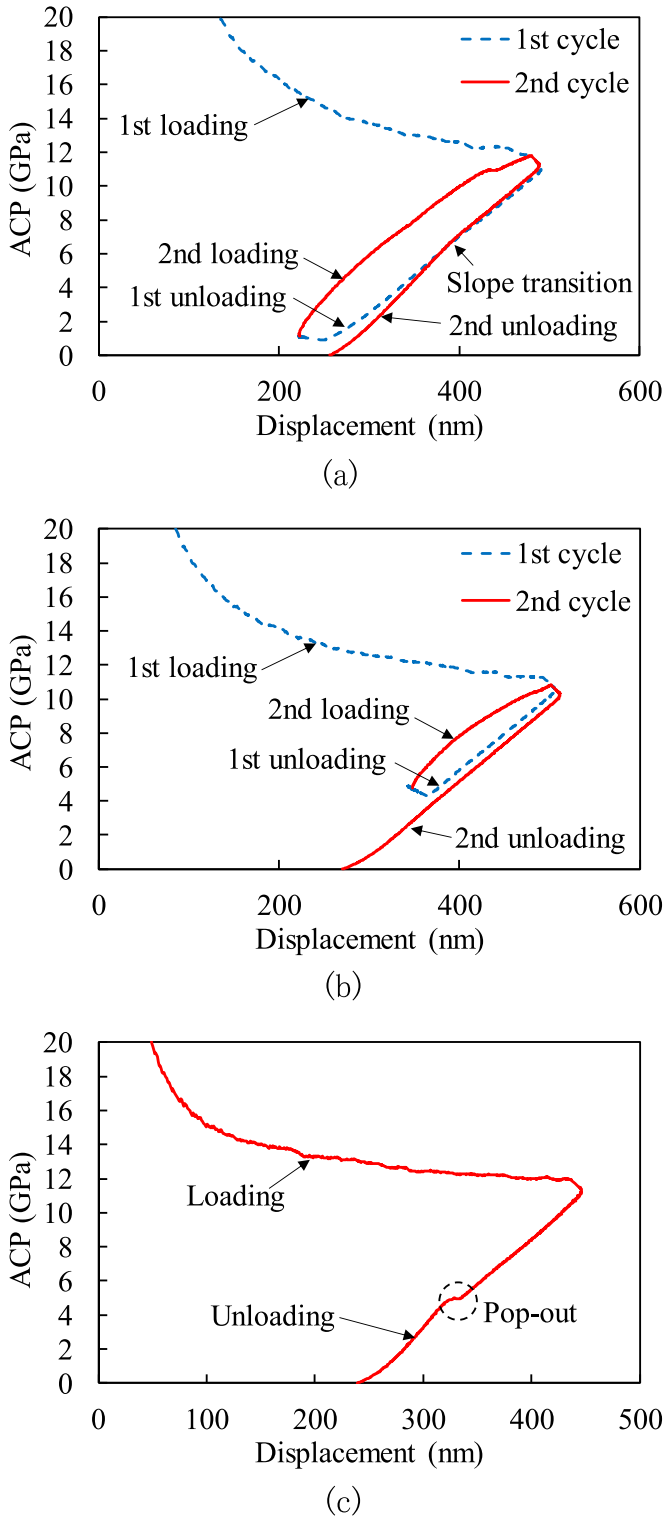

Figure 13. Average contact pressure during each indentation corresponding to (a) ~ (c) in figure 12.

accepted that the pop-out is a result of momentary volume increase by wide phase transformation under well-lowered pressure. Phase transformation by random nucleation and growth of seeds progresses on the 1st part of unloading. Around the pop-out pressure, the catastrophic phase transformation from the seeds is triggered with large volume expansion causing a pop-out. After the catastrophic phase transformation, no region that shows phase transformation is left. As a result, a subsequent faster ACP decrease follows by only elastic recovery, which caused slope transition via the pop-out.

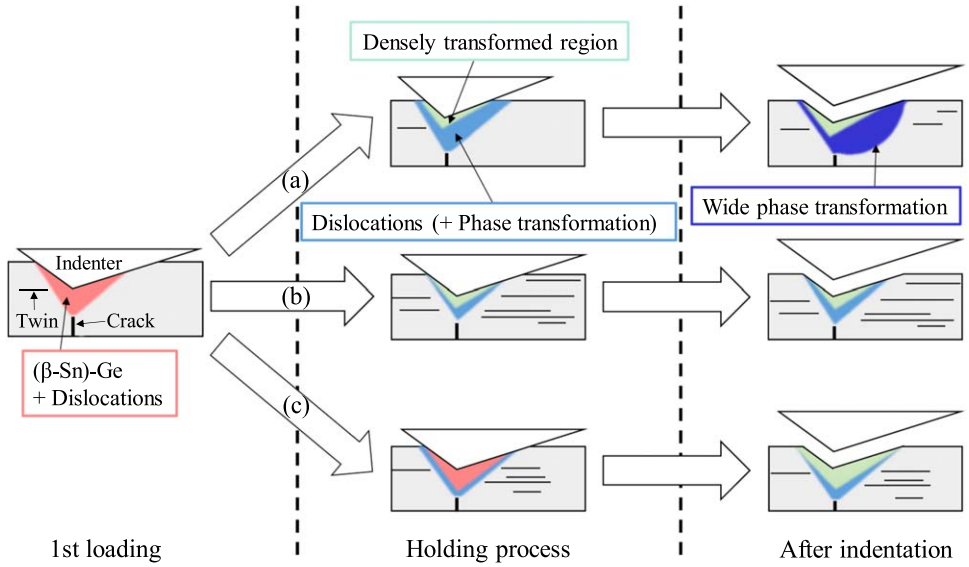

Figure 14. Diagram of phase transformation behaviors during multi-cyclic nanoindentation depending on holding load ΔP; (a) low ΔP; (b) middle ΔP; (c) high ΔP.

3.5. Phase transformation paths

According to the aforementioned results and discussion, phase transformation pathways of single-crystal Ge during multi-cyclic nanoindentation can be classified as figure 14. At the 1st loading, dc-Ge transforms to intermediate (β-Sn)-Ge by pressure. Dislocations are also generated as observed in TEM images. For the case of a low ΔP (path (a) in figure 14), the (β-Sn)-Ge transforms to other phases on the subsequent unloading before the holding process. At this step, phase transformation may not be a dominant behavior because the process is almost the same as single indentation showing a middle fraction in figure 2. During the holding process, few twins are formed by low pressure. Therefore, the wide surrounding region demonstrates further phase transformation to r8-Ge by the 2nd loading/unloading. The wide transformed region as observed in figure 6 resulted in the high fraction of r8-Ge appearance in figure 2. For indentation with a middle ΔP (path (b) in figure 14), on the other hand, relatively high pressure is constantly added during the holding process. This generates quite a few and wide twins. As a result, phase transformation on the 2nd cycle is prevented by the twins, which lowered the r8-Ge appearance on Raman spectra as figure 2. For a high ΔP (path (c) in Figure 14), (β-Sn)-Ge formed on the 1st loading is sustained during the holding process because of little or no unloading. In the (β-Sn)-Ge layer, stress is accumulated. This subsequently causes a wide formation of a densely transformed region containing r8-Ge and st12-Ge, although twins may also be formed in the surrounding region.

4. Conclusions

Multi-cyclic nanoindentation was performed on single-crystal Ge with different holding loads ΔP and resulting phase transformation behaviors were investigated. Cross-sectional TEM observation of the indents revealed distinctly different phase transformation behaviors depending on ΔP. For a low ΔP, the r8-Ge phase containing dislocations was widely formed around the indent. For a middle ΔP, significant twin nucleation occurred without phase transformation. In contrast, a high ΔP resulted in a remarkably greater transformation region generated from (β-Sn)-Ge by high stress accumulation. Pressure analysis using ACP provided kinetic evidence for the above-mentioned phase transformation mechanisms. Due to the phase transformation-induced volume expansion, a slope transition of ACP and a pop-out were confirmed during the last unloading process. Based on these results, phase transformation pathways during multi-cyclic nanoindentation were identified, which enhances the understanding of the nanoscale mechanical response of single-crystal Ge under complicated loads.

ORCID iDs

Jiwang Yan https://orcid.org/0000-0002-5155-3604

References

[1] Jamieson J C 1963 Crystal structures at high pressures of metallic modifications of silicon and germanium *Science (80-.)* **139** 762–4
[2] Minomura S and Drickamer H G 1962 Pressure induced phase transitions in silicon, germanium and some III–V compounds *J. Phys. Chem. Solids* **23** 451–6
[3] Gerk A P and Tabor D 1978 Indentation hardness and semiconductor–metal transition of germanium and silicon *Nature* **271** 732–3
[4] Pharr G M *et al* 1992 Electrical resistance of metallic contacts on silicon and germanium during indentation *J. Mater. Res.* **7** 961–72
[5] Nelmes R J, McMahon M I, Wright N G, Allan D R and Loveday J S Stability and crystal structure of BC8 germanium *Phys. Rev.* B **48** 9883–61993
[6] Deshmukh S *et al* 2014 Phase transformation pathways in amorphous germanium under indentation pressure *J. Appl. Phys.* **115** 153502
[7] Oliver D J, Bradby J E, Williams J S, Swain M V and Munroe P 2009 Rate-dependent phase transformations in nanoindented germanium *J. Appl. Phys.* **105** 126101
[8] Jang J, Lance M J, Wen S and Pharr G M 2005 Evidence for nanoindentation-induced phase transformations in germanium *Appl. Phys. Lett.* **86** 131907
[9] Haberl B *et al* 2014 Controlled formation of metastable germanium polymorphs *Phys. Rev.* B **89** 144111
[10] Bradby J E, Williams J S, Wong-Leung J, Swain M V and Munroe P 2002 Nanoindentation-induced deformation of Ge *Appl. Phys. Lett.* **80** 2651–3
[11] Johnson B C *et al* 2013 Evidence for the R8 Phase of Germanium *Phys. Rev. Lett.* **110** 085502
[12] Williams J S *et al* 2013 Hexagonal germanium formed via a pressure-induced phase transformation of amorphous germanium under controlled nanoindentation *Phys. Status Solidi—Rapid Res. Lett.* **7** 355–9
[13] Xiao S and Pirouz P 1992 On diamond-hexagonal germanium *J. Mater. Res.* **7** 1406–12
[14] Gogotsi Y G, Domnich V, Dub S N, Kailer A and Nickel K G 2000 Cyclic nanoindentation and Raman microspectroscopy study of phase transformations in semiconductors *J. Mater. Res.* **15** 871–9
[15] Kosai K, Huang H and Yan J 2017 Comparative study of phase transformation in single-crystal germanium during single and cyclic nanoindentation *Crystals* **7** 333
[16] Kosai K and Yan J 2018 Investigation of subsurface damage behaviors in single-crystal Ge by multi-cyclic nanoindentation *Procedia CIRP* **71** 244–8
[17] Kailer A, Nickel K G and Gogotsi Y G 1999 Raman microspectroscopy of nanocrystalline and amorphous phases in hardness indentations *J. Raman Spectrosc.* **30** 939–46
[18] Clarke D R, Kroll M C, Kirchner P D, Cook R F and Hockey B J 1988 Amorphization and conductivity of silicon and germanium induced by indentation *Phys. Rev. Lett.* **60** 2156–9
[19] Haberl B, Bayu Aji L B, Williams J S and Bradby J E 2012 The indentation hardness of silicon measured by instrumented indentation: what does it mean? *J. Mater. Res.* **27** 3066–72
[20] Bradby J E, Williams J S, Wong-Leung J, Swain M V and Munroe P 2000 Transmission electron microscopy observation of deformation microstructure under spherical indentation in silicon *Appl. Phys. Lett.* **77** 3749–51
[21] Haq A J and Munroe P R 2009 Phase transformations in (111) Si after spherical indentation *J. Mater. Res.* **24** 1967–75
[22] Bradby J E, Williams J S, Wong-Leung J, Swain M V and Munroe P 2001 Mechanical deformation in silicon by micro-indentation *J. Mater. Res.* **16** 1500–7
[23] Domnich V, Gogotsi Y and Dub S 2000 Effect of phase transformations on the shape of the unloading curve in the nanoindentation of silicon *Appl. Phys. Lett.* **76** 2214–6
[24] Wong S, Haberl B, Williams J S and Bradby J E 2015 The influence of hold time on the onset of plastic deformation in silicon *J. Appl. Phys.* **118** 245904
[25] Juliano T, Gogotsi Y and Domnich V 2003 Effect of indentation unloading conditions on phase transformation induced events in silicon *J. Mater. Res.* **18** 1192–201
[26] Huang H and Yan J 2015 On the mechanism of secondary pop-out in cyclic nanoindentation of single-crystal silicon *J. Mater. Res.* **30** 1861–8
[27] Huang H and Yan J 2015 New insights into phase transformations in single crystal silicon by controlled cyclic nanoindentation *Scr. Mater.* **102** 35–8
[28] Huang H and Yan J 2016 Volumetric and timescale analysis of phase transformation in single-crystal silicon during nanoindentation *Appl. Phys.* A **122** 607
[29] Jian S-R, Chen G-J and Juang J-Y 2010 Nanoindentation-induced phase transformation in (110)-oriented Si single-crystals *Curr. Opin. Solid State Mater. Sci.* **14** 69–74
[30] Huston L Q, Kiran M S R N, Smillie L A, Williams J S and Bradby J E 2017 Cold nanoindentation of germanium *Appl. Phys. Lett.* **111** 021901
[31] Novikov N V, Dub S N, Milman Y V, Gridneva I V and Chugunova S I 1996 Application of nanoindentation method to study a semiconductor-metal phase transformation in silicon *J. Superhard Mater.* **18** 32
[32] Jang J and Pharr G M 2008 Influence of indenter angle on cracking in Si and Ge during nanoindentation *Acta Mater.* **56** 4458–69
[33] Siethoff H, AhlbornSiethoff K and Schröter W 1999 New analysis of the yield point of germanium *Phys. Status Solidi* **174** 205–12
[34] Ruffell S, Bradby J E, Williams J S and Munroe P 2007 Formation and growth of nanoindentation-induced high pressure phases in crystalline and amorphous silicon *J. Appl. Phys.* **102** 063521
[35] Menoni C S, Hu J Z and Spain I L 1986 Germanium at high pressures *Phys. Rev.* B **34** 362–8
[36] Malone B D and Cohen M L 2012 Electronic structure, equation of state, and lattice dynamics of low-pressure Ge polymorphs *Phys. Rev.* B **86** 054101